



EVA-NET: INTERPRETABLE BRAIN AGE PREDICTION VIA CONTINUOUS AGING PROTOTYPES FROM EEG

Kunyu Zhang^{1,2}

**Department of Neurosurgery, Qilu Hospital of
Shandong University
Arizona State University**

Xiangjie Shi⁴

**University of Science and
Technology Beijing**

Mingxuan Wang³

Zhengzhou University

Haoxing Xu⁵

**Southern University of
Science and Technology**

Chao Zhang¹

Department of Neurosurgery, Qilu Hospital of Shandong University

chao_zhang@sdu.edu.cn

ABSTRACT

The brain age is a key indicator of brain health. While electroencephalography (EEG) is a practical tool for this task, existing models struggle with the common challenge of imperfect medical data, such as learning a “normal” baseline from weakly supervised, healthy-only cohorts. This is a critical anomaly detection task for identifying disease, but standard models are often black boxes lacking an interpretable structure. We propose EVA-Net, a novel framework that recasts brain age as an interpretable anomaly detection problem. EVA-Net uses an efficient, sparsified-attention Transformer to model long EEG sequences. To handle noise and variability in imperfect data, it employs a Variational Information Bottleneck to learn a robust, compressed representation. For interpretability, this representation is aligned to a continuous prototype network that explicitly learns the normative healthy aging manifold. Trained on 1297 healthy subjects, EVA-Net achieves state-of-the-art accuracy. We validated its anomaly detection capabilities on an unseen cohort of 27 MCI and AD patients. This pathological group showed significantly higher brain-age gaps and a novel Prototype Alignment Error, confirming their deviation from the healthy manifold. EVA-Net provides an interpretable framework for healthcare intelligence using imperfect medical data.

1 Introduction

Brain age (BA) aims to estimate an individual’s biological age of the brain from neural data, and the difference between the estimated BA and chronological age, known as the brain-age gap (BAG), serves as a compact indicator of brain health and aging velocity [1–3]. Compared with structural or functional neuroimaging pipelines, electroencephalography (EEG) offers practical advantages in cost, accessibility, wearability, and longitudinal monitoring, while directly capturing fast neural dynamics [4–6]. These properties position EEG-based BA modeling as a complementary route to imaging-based approaches for population-level health assessment and individual risk stratification, and make it well-suited for tracking functional changes related to aging, lifestyle, and interventions.

Despite promising progress, current EEG BA studies face several methodological bottlenecks [7]. First, efficient long-range temporal modeling remains limited: many methods rely on short windows or local convolutions and therefore struggle to capture multi-scale dynamics spanning instantaneous waveforms to segment-level rhythms under tractable computation. Second, robustness and cross-domain generalization are challenged by device, site, and subject variability [8]. Standard models trained on single-source data often overfit to site-specific noise and artifacts [9], which impairs their transferability to external clinics. EEG is sensitive to these distribution shifts, challenging stability on unseen data. Third, and most critically for real-world application, standard methods fail to address the challenge of imperfect medical data, such as learning from one-class (e.g., healthy-only) cohorts. This is a form

of anomaly detection for disease detection using imperfect data, where the goal is not just regression, but to define a tight, interpretable boundary of “normal” aging. Current end-to-end models lack an explicit “ideal healthy aging trajectory,” making it difficult to perform principled anomaly detection or interpret the BAG as a true deviation from health, rather than just statistical noise.

To address these issues, we propose a unified framework that recasts brain age prediction as a weakly supervised anomaly detection task [10, 11], designed to operate on imperfect (healthy-only) medical data. Concretely, short-window EEG epochs are first transformed via temporal embedding into a sequence representation amenable to efficient attention [12]. A sparsified long-sequence attention backbone then captures multi-scale dependencies without sacrificing temporal coverage. In the latent space, a variational information bottleneck (VIB) enhances robustness by suppressing age-irrelevant factors linked to subject- or device-specific variability. This acts as a regularization mechanism that forces the model to ‘forget’ site-specific nuisance variables from the training source, thereby preserving intrinsic aging patterns that are transferable to unseen domains. We further introduce an age-conditioned continuous prototype network that maps scalar age onto a smooth, normative healthy trajectory in latent space [13]. An alignment constraint pulls healthy sample embeddings toward their age-conditioned prototypes, endowing the representation with an explicit geometrical structure for “normal” age. This transforms the model into a powerful anomaly detector [14], where pathological states (e.g., AD) can be identified and quantified as significant deviations from this interpretable healthy manifold.

The main contributions of this work are as follows:

- **Efficient long-sequence temporal modeling.** We employ a sparsified long-sequence attention encoder as the backbone to unify multi-scale dependencies from instantaneous waveforms to segment-level rhythms, offering a large receptive field under tractable computation and avoiding the fragmentation of short-window processing.
- **Robust representation via a variational information bottleneck.** We impose an explicit information-throughput constraint in the latent space to suppress age-irrelevant subject/device factors and noise. This enforces a selective compression of healthy age-related features, yielding a robust representation of normative aging and ensuring the learned manifold is not contaminated by non-age-related variance when learning from imperfect (healthy-only) medical data.
- **Age-conditioned continuous prototype alignment.** We construct a continuous “normative healthy aging trajectory” by mapping scalar age into the latent space and align sample embeddings to their age-conditioned prototypes. This enforces a smooth, interpretable geometry for healthy aging, transforming the task into a weakly supervised anomaly detection problem where the BAG serves as a principled measure of deviation from the normative manifold.

- **Validation as an Anomaly Detector.** Across strong baselines and diverse data settings, our method achieves *overall superior* performance in accuracy and robustness. We further validate our model’s utility as an anomaly detector by demonstrating that an unseen cohort of AD patients shows a significantly larger BAG, confirming their deviation from the learned healthy aging manifold.

2 Related Work

2.1 Deep learning for brain age prediction

Brain age (BA) and the brain-age gap (BAG) have been widely explored using deep learning in neuroimaging [1, 2, 15]. CNNs capture morphometric patterns, graph models encode region interactions, and Transformers aggregate multi-scale context [16]. Recent advances include multimodal imaging fusion [17] and disease-specific models [18, 19]. However, most rely on mixed cohorts or case-control designs. Few address learning normative trajectories from healthy-only cohorts, essential for defining a baseline to detect pathological deviations [3]. Imaging approaches also face cost and accessibility constraints. Our work leverages efficient long-sequence attention for EEG, designed for normative modeling and anomaly detection.

2.2 Development of EEG-based brain age prediction

EEG-based BA research combines handcrafted features with regressors, end-to-end learning via CNNs and spatiotemporal graphs [20, 21], and robustness techniques including domain adaptation [22]. Transformers have captured long-range dependencies [23–25]. Three challenges remain for anomaly detection from imperfect data: (i) efficient long-range temporal modeling; (ii) resilience to distribution shifts; and (iii) lack of latent geometry reflecting normative aging, preventing BAG interpretation as an anomaly score. We address these with a sparsified encoder (i), variational information bottleneck (ii), and age-conditioned prototype network (iii).

2.3 Explainability and latent-space structure

Explainability for BA models includes saliency visualizations, prototype-based approaches [26, 27], and latent-space regularization. The Information Bottleneck (IB) [28, 29] learns compressed representations retaining task-relevant information and has been applied to brain disorder diagnosis [30]. The Variational Information Bottleneck (VIB) [31] extends this via tractable variational formulation for weakly-supervised tasks [32]. However, most strategies remain post hoc and lack continuous healthy age manifolds for BAG interpretation. Recent normative modeling [33] explores generative manifold learning. Our framework integrates explanation into design: VIB enforces compression, and age-conditioned prototypes shape latent space into a smooth healthy aging trajectory, providing interpretable anomaly detection.

3 Methodology

In this section, we present **EVA-Net**, a novel deep learning Efficient Variational Alignment Network designed to learn a robust and interpretable normative manifold of healthy brain aging, as shown in Figure 1. The overall architecture comprises three key components: (1) an Efficient long-sequence encoder with ProbSparse attention to capture multi-scale temporal dependencies; (2) a Variational Information Bottleneck (VIB) to learn a compressed and robust representation Z_i by suppressing age-irrelevant noise; and (3) an Alignment module with an age-conditioned continuous prototype network (P_y) that provides an interpretable structure for healthy aging. By jointly optimizing for prediction accuracy, representation compression (L_{IB}), and prototype alignment (L_{align}), EVA-Net enables the robust and interpretable detection of anomalies as deviations from the learned healthy manifold.

3.1 Problem Formulation

Our objective is to learn a normative model of healthy brain aging from a training set $D_{train} = \{(X_i, y_i)\}_{i=1}^N$ of N healthy subjects. The input $X_i \in \mathbb{R}^{C \times T}$ is a 19-channel, 4-second (T=1000) EEG epoch, and $y_i \in \mathbb{R}^+$ is the chronological age. Our framework, EVA-Net, is trained to learn three functions simultaneously: (1) an efficient probabilistic encoder E_ϕ (Informer-VIB backbone) that maps X_i to a robust latent representation $Z_i \in \mathbb{R}^d$ by optimizing for efficiency (ProbSparse) and robustness (VIB); (2) a continuous prototype network P_θ that maps a true scalar age y to its corresponding ideal prototype $P_y \in \mathbb{R}^d$ in the same latent space; and (3) a prediction head f_ψ that regresses age $\hat{y}_i = f_\psi(Z_i)$. All parameters $\{\phi, \theta, \psi\}$ are jointly optimized via a composite loss $L_{Total} = L_{pred} + \beta L_{IB} + \gamma L_{align}$ to balance prediction accuracy, information compression, and geometric alignment. For anomaly detection, this allows us to compute both the standard Brain-Age Gap (BAG, $\hat{y} - y$) and a novel Prototype Alignment Error (PAE, $\|Z - P_y\|_2$) as an interpretable measure of deviation from the learned healthy manifold.

3.2 Efficient Long-Sequence Encoder

The first component processes input $X_i \in \mathbb{R}^{C \times T}$ ($C = 19$ channels, $T = 1000$ time-points). Standard Transformer self-attention

$$\mathcal{A}(Q, K, V) = \text{Softmax}\left(\frac{QK^T}{\sqrt{d_k}}\right)V, \quad (1)$$

requires $O(T^2)$ computation, prohibitive for $T = 1000$. Channel-wise features are projected to d_{model} with sinusoidal positional encoding, yielding $S_i \in \mathbb{R}^{T \times d_{model}}$.

The **ProbSparse** attention reduces complexity to $O(T \log T)$ (Figure 2) by selecting queries with high KL divergence from uniform attention. Query importance is

approximated by:

$$\bar{M}(q_i, K) = \max_j \left\{ \frac{q_i k_j^T}{\sqrt{d_k}} \right\} - \frac{1}{T} \sum_{j=1}^T \frac{q_i k_j^T}{\sqrt{d_k}} \quad (2)$$

We select the top $u = c \cdot \ln T$ queries to form sparse set \hat{Q} , computing attention only for this subset:

$$\mathbf{A}_{ProbSparse}(Q, K, V) = \text{Softmax}\left(\frac{\hat{Q}K^T}{\sqrt{d_k}}\right)V \quad (3)$$

After L encoder layers, global average pooling produces hidden representation $H_i \in \mathbb{R}^{d_{model}}$.

3.3 Variational Information Bottleneck

The hidden representation $H_i \in \mathbb{R}^{d_{model}}$ produced by the efficient encoder, while compact, may still contain substantial age-irrelevant information, such as subject-specific, site-specific, or noise-related features inherent in imperfect medical data. To enhance robustness and generalization, we introduce a Variational Information Bottleneck (VIB) as a probabilistic regularizer. This module ensures that the final latent representation Z_i is selectively compressed to retain only the minimal information necessary for age prediction.

Instead of a deterministic mapping, we treat H_i as the input to a stochastic encoder that parameterizes a posterior distribution $q_\phi(Z_i|X_i)$, which we approximate as a Gaussian $\mathcal{N}(\mu_i, \sigma_i^2)$. The mean $\mu_i \in \mathbb{R}^d$ and log-variance $\log \sigma_i^2 \in \mathbb{R}^d$ (where d is the latent dimension) are computed via two separate linear heads applied to H_i :

$$\mu_i = W_\mu H_i + b_\mu \quad \text{and} \quad \log \sigma_i^2 = W_\sigma H_i + b_\sigma \quad (4)$$

To enable backpropagation, we use the reparameterization trick to sample the final latent vector $Z_i \in \mathbb{R}^d$:

$$Z_i = \mu_i + \sigma_i \odot \epsilon, \quad \text{where } \epsilon \sim \mathcal{N}(0, I) \quad (5)$$

This stochastic encoding introduces a new objective to the total loss function: the Information Bottleneck loss, L_{IB} . This loss is the KL divergence between the learned posterior $q_\phi(Z_i|X_i)$ and a standard Gaussian prior $p(Z) = \mathcal{N}(0, I)$. This L_{IB} term, defined as:

$$L_{IB} = D_{KL}(q_\phi(Z_i|X_i)||p(Z)) = \frac{1}{2} \sum_{j=1}^d (\sigma_{i,j}^2 + \mu_{i,j}^2 - \log \sigma_{i,j}^2 - 1) \quad (6)$$

acts as a powerful regularizer. It penalizes the information throughput, forcing the encoder to discard the non-essential variations in X_i (noise, artifacts, subject ID) and produce a maximally compressed, robust representation Z_i focused solely on healthy aging.

3.4 Continuous Prototype Alignment

The VIB module ensures the latent representation Z_i is robust and compressed. However, it does not guarantee

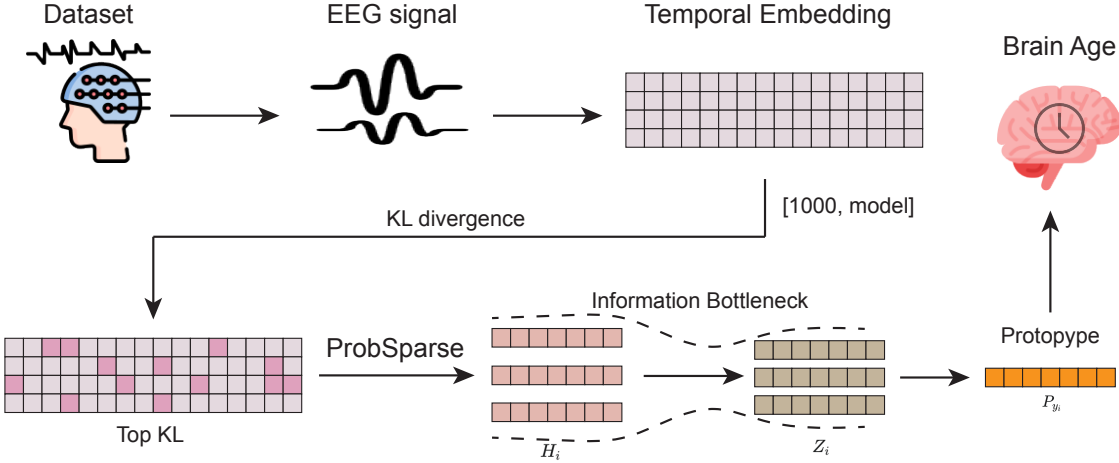


Figure 1: The overall architecture of our proposed EVA-Net. EEG signals are converted via Temporal Embedding into a sequence. An efficient backbone (using ProbSparse attention by identifying Top KL time-points) extracts a hidden state H_i . This state is passed through an Information Bottleneck (VIB) to produce a robust latent code Z_i . Z_i is then used for both Brain Age prediction (regression) and alignment with an ideal age-matched Prototype P_{y_i} .

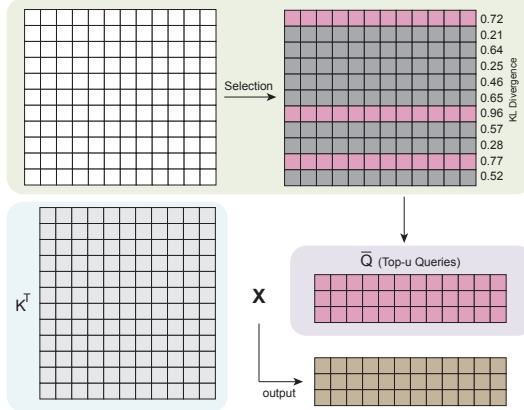


Figure 2: ProbSparse attention mechanism achieving $O(L \log L)$ complexity. Queries are ranked by KL divergence scores, with top-scoring queries (pink) forming sparse matrix \bar{Q} . Computing $\bar{Q}K^T$ bypasses full $L \times L$ attention, reducing computational cost while preserving critical temporal dependencies.

that the latent space is well-structured; the representations of subjects with similar ages (e.g., 60 and 61) are not explicitly encouraged to be close to each other. To address this and endow the model with a clear, interpretable geometry, we introduce the Alignment component: an age-conditioned continuous prototype network, P_θ , parameterized by θ .

This independent network P_θ is designed to learn the “ideal” manifold of healthy aging by mapping a scalar chronological age $y \in \mathbb{R}^+$ to its corresponding “ideal” proto-

tope $P_y \in \mathbb{R}^d$ in the same latent space as Z_i . A simple scalar age is a poor input for a neural network; therefore, we first encode y_i into a high-dimensional vector y_i^{embed} using a sinusoidal (Fourier) positional encoding, analogous to that used in Transformers. This age embedding is then passed through P_θ , which is implemented as a small Multi-Layer Perceptron (MLP):

$$P_{y_i} = P_\theta(y_i^{embed}) \quad (7)$$

To enforce the geometric structure, we introduce a loss term, the prototype alignment loss L_{align} . This loss acts as a “pulling” force, compelling the probabilistic encoder E_ϕ to map its sample representation Z_i to be close to the ideal prototype P_{y_i} defined by the prototype network. We define this loss as the Mean Squared Error (MSE) between the two vectors:

$$L_{align} = \|Z_i - P_{y_i}\|_2^2 \quad (8)$$

This alignment loss is critical, as it forces the encoder E_ϕ and the prototype network P_θ to jointly discover a latent space where the “ideal” healthy aging trajectory P_y is continuous and monotonic, and where the “real” (and noisy) sample embeddings Z_i are anchored to their respective positions along this normative manifold.

3.5 Training Objective and Composite Loss

The EVA-Net framework is trained end-to-end by jointly optimizing all three components: the efficient encoder E_ϕ , the prototype network P_θ , and a final prediction head f_ψ . The prediction head is a simple Multi-Layer Perceptron (MLP) that takes the robust latent vector $Z_i \in \mathbb{R}^d$ (from the VIB module) as input and regresses the final scalar brain age \hat{y}_i :

$$\hat{y}_i = f_\psi(Z_i) \quad (9)$$

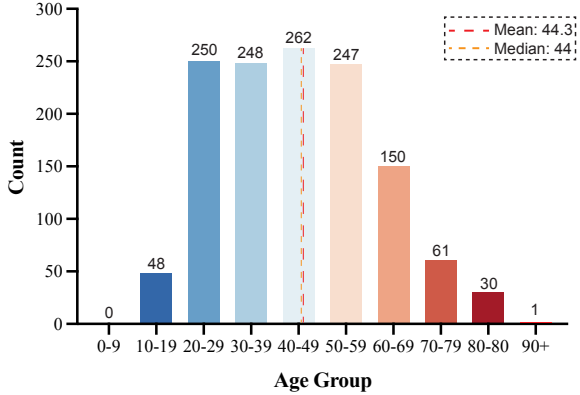


Figure 3: Age distribution of the normative healthy cohort. A bar chart illustrating the sample count by decade. The distribution is concentrated in adulthood, and fewer subjects in the younger and older brackets, with a cohort mean age of 44.3 years and a median age of 44 years.

Our full training objective is a composite loss L_{Total} designed to simultaneously balance three distinct goals: prediction accuracy, representation robustness, and latent space interpretability. This loss is the weighted sum of the three corresponding loss terms:

$$L_{Total} = L_{pred} + \beta \cdot L_{IB} + \gamma \cdot L_{align} \quad (10)$$

where β and γ are hyperparameters that balance the contribution of each component.

The first term, L_{pred} , is the primary task objective, ensuring the latent representation Z_i contains sufficient information to accurately predict age. We define this as the Mean Squared Error (MSE) between the predicted age and the true chronological age:

$$L_{pred} = \frac{1}{N} \sum_{i=1}^N (\hat{y}_i - y_i)^2 \quad (11)$$

The second term, L_{IB} , is the KL divergence loss from the VIB module (defined in Eq. 6). This term acts as an information-theoretic regularizer, penalizing the model for encoding age-irrelevant information and thus enhancing the robustness and generalization of Z_i . The third term, L_{align} , is the prototype alignment loss (defined in Eq. 8). This loss compels the encoder to map samples onto a structured, continuous manifold that aligns with the “ideal” healthy aging trajectory learned by the prototype network P_θ . By jointly optimizing this composite loss, EVA-Net learns a latent space that is not only predictive and robust, but also geometrically interpretable.

4 Experiments

4.1 Datasets

This study was conducted in accordance with the Declaration of Helsinki and was approved by the Ethics Committee

of Qilu Hospital of Shandong University (Protocol Number: KYLL-202406 (YJ)-010). Written informed consent was obtained from all subjects or their legal guardians involved in the study.

All data were acquired from Qilu Hospital of Shandong University and divided into two distinct cohorts to train and evaluate our normative modeling framework. The primary “normative” cohort consists of 1297 healthy subjects selected based on clinical reports documenting a “normal” EEG and the absence of any neurological or psychiatric disorders. As shown in Figure 3, this cohort has a mean chronological age of 44.3 years and a median of 44 years. The age distribution is not uniform; it is heavily concentrated in adulthood (20-59 years), with fewer subjects in the pediatric (10-19) and elderly (60+) age brackets. The second “pathological” cohort, used for out-of-distribution anomaly detection, comprises 27 subjects with cognitive impairment: 12 with Mild Cognitive Impairment (MCI) and 15 with Alzheimer’s Disease (AD).

All recordings from both cohorts were processed through an identical, standardized preprocessing pipeline (detailed in Section 4.2) to produce 19-channel, 4-second EEG epochs ($X_i \in \mathbb{R}^{19 \times 1000}$). To robustly evaluate model performance on the 1297-subject healthy cohort, we employed a 10-fold cross-validation strategy. The cohort was randomly partitioned into 10 equal, non-overlapping folds. In each of the 10 iterations (folds), one fold was reserved as the healthy test set, and the remaining nine folds were used as the training set to learn the EVA-Net parameters $\{\phi, \theta, \psi\}$. The final regression performance on healthy data is reported as the average and standard deviation of the metrics across all 10 folds. The 27 MCI and AD subjects are used as a separate test set to evaluate the model’s ability to detect pathological deviations from the healthy norm.

4.2 Data Preprocessing

All data from both the healthy and pathological cohorts underwent an identical, standardized preprocessing pipeline implemented using MNE-Python. First, raw data was loaded from CSV, units were converted to Volts, and only the 19 standard 10-20 EEG channels were retained. Bad channels were automatically detected based on abnormal variance and low inter-channel correlation criteria and subsequently repaired using spherical spline interpolation. The data was then re-referenced to a common average reference (AR) and temporally filtered using a 0.5-45 Hz FIR band-pass filter and a 60 Hz notch filter to remove signal drifts and powerline noise. Ocular, muscular, and cardiac artifacts were automatically identified and removed using FastICA, with artifactual components selected based on their high correlation (threshold: 0.3) with frontal (FP1, FP2) channels. Finally, the cleaned, continuous signal was epoched into 4-second non-overlapping windows. Any epochs with a peak-to-peak amplitude exceeding a 150 μ V threshold were automatically discarded, and the resulting

clean epochs (tensors of shape ‘[19, 1000]’) were stored and used for all subsequent model training and evaluation.

4.3 Baselines

We benchmark the performance of our proposed EVA-Net against a comprehensive suite of competitive baselines, all trained and evaluated on the same preprocessed datasets and 10-fold cross-validation splits. These baselines are categorized into three groups: (1) two widely-used time series models, EEGNet [34] and a Temporal Convolutional Network (TCN) [35]; (2) two state-of-the-art (SOTA) EEG representation models, DEEP-EMD [36] and WST [37]; and (3) two recent models specifically designed for brain age prediction, NCV [38] and MBN [39]. All baseline models were re-implemented, and their experiments were conducted following the settings described in their respective original publications.

4.4 Implementation Details

Our EVA-Net framework was implemented in PyTorch. All experiments are conducted on an NVIDIA RTX 4090 GPU. The efficient encoder backbone was configured with $L = 4$ Informer layers, a model dimension of $d_{model} = 128$, and $H = 8$ attention heads. The ProbSparse attention sampling factor c was set to 5. The VIB module projected the $d_{model} = 128$ hidden state H_i into a latent dimension of $d = 64$, producing μ_i and $\log \sigma_i^2$. The continuous prototype network P_θ and the prediction head f_ψ were both implemented as 3-layer MLPs with ReLU activations, with P_θ mapping the encoded age to $d = 64$ and f_ψ mapping Z_i to a single scalar output. All models were trained for 200 epochs using the AdamW optimizer with a learning rate of $1e - 4$, a weight decay of $1e - 5$, and a batch size of 64. A cosine annealing scheduler was used to adjust the learning rate. We applied early stopping with a patience of 20 epochs based on the validation set’s L_{pred} loss. The loss hyperparameters were set to $\beta = 1e - 3$ for the L_{IB} loss and $\gamma = 0.7$ for the L_{align} loss based on empirical tuning on the validation set.

4.5 Evaluation Metrics

Our evaluation protocol is twofold, designed to assess both standard regression accuracy on healthy individuals and the model’s capability for anomaly detection. **(1) Normative Regression Performance:** We evaluate the model’s prediction accuracy on the healthy test folds from our 10-fold cross-validation. For this “healthy person prediction standard,” we report the average and standard deviation of three core regression metrics: the Mean Absolute Error (MAE), the Root Mean Squared Error (RMSE), and the R-squared (R^2) score to measure the proportion of variance explained by the model’s predictions. **(2) Anomaly Detection Efficacy:** We then evaluate the model’s ability to distinguish the pathological cohort (12 MCI and 15 AD subjects) from the healthy test subjects. For this, we formally define the two metrics introduced in our Prob-

lem Formulation. The first is the standard Brain-Age Gap (BAG), calculated as the predicted age \hat{y} (from f_ψ) minus the chronological age y :

$$\text{BAG} = \hat{y} - y \quad (12)$$

The second is our proposed Prototype Alignment Error (PAE), which quantifies an individual’s deviation from the learned healthy manifold as the Euclidean distance between their latent embedding Z (from E_ϕ) and their age-matched ideal prototype P_y (from P_θ):

$$\text{PAE} = \|Z - P_y\|_2 \quad (13)$$

We hypothesize that the MCI and AD cohorts will show significantly higher mean BAG and PAE values, quantifying their deviation from the learned normative manifold. We use two-sample t-tests to confirm the statistical significance of these differences.

5 Results

5.1 Performance Comparison

We present the results of the proposed EVA-Net and all baseline models on the primary task of normative age regression, evaluated on the 10% held-out healthy test sets from our 10-fold cross-validation.

Table 1 summarizes the performance according to the MAE, RMSE, and R^2 metrics. Our proposed EVA-Net achieves state-of-the-art performance, outperforming all competitive baselines on all three metrics. Notably, EVA-Net achieves an MAE of 2.645, a 13.4% improvement over the strongest baseline, MBN (MAE of 3.053). Similarly, EVA-Net obtains the lowest RMSE (3.327) and the highest R^2 (0.939), indicating that its predictions are not only accurate but also explain a larger proportion of the variance in chronological age.

5.2 Ablation Study

To validate the contribution of each key component in our proposed EVA-Net framework, we conducted a comprehensive ablation study. We evaluated three distinct variants of our model on the 10-fold cross-validation dataset:

- **EVA-Net w/o E (Efficient):** In this variant, we removed the (E)fficient ProbSparse attention backbone. We replaced the Informer-based encoder with a standard GRU-based recurrent neural network to model the temporal sequence, while keeping the VIB and Alignment components.
- **EVA-Net w/o V (Variational):** We removed the (V)ariational Information Bottleneck. The hidden representation H_i from the efficient encoder was passed directly and deterministically to the prediction head f_ψ and the prototype alignment L_{align} . The L_{IB} loss term was removed from the training objective.
- **EVA-Net w/o A (Alignment):** We removed the (A)lignment component entirely. The continuous prototype network P_θ was removed, and the L_{align} loss was

Table 1: Performance comparison on the held-out healthy test set. Results are averaged across the 10-fold cross-validation. For MAE and RMSE, lower is better (\downarrow). For R^2 , higher is better (\uparrow). Best results are highlighted in bold.

Metric	EEGNet	TCN	Deep-EMD	WST	NCV	MBN	EVA-Net (Ours)
MAE \downarrow	6.435	4.924	3.497	3.176	5.172	3.053	2.645
RMSE \downarrow	9.267	6.137	4.196	4.469	6.724	3.664	3.327
$R^2 \uparrow$	0.836	0.891	0.933	0.935	0.857	0.936	0.939

Table 2: Ablation study of EVA-Net’s core components. Results are averaged across the 10-fold cross-validation on the healthy test set. The full model’s performance is compared against variants lacking the Efficient backbone (w/o E), the Variational bottleneck (w/o V), and the Alignment loss (w/o A).

Model Variant	MAE \downarrow	RMSE \downarrow	$R^2 \uparrow$
EVA-Net (Full Model)	2.645	3.327	0.939
EVA-Net w/o E (Efficient)	5.138	6.350	0.881
EVA-Net w/o V (Variational)	5.512	7.104	0.866
EVA-Net w/o A (Alignment)	5.903	7.822	0.849

omitted. The model was trained only to optimize the prediction and VIB losses ($L_{pred} + \beta L_{IB}$).

The results, presented in Table 2, demonstrate the critical and synergistic role of all three components. The full EVA-Net (MAE 2.645) significantly outperforms all ablated models. The removal of any single component, Efficient, Variational, or Alignment, causes a catastrophic drop in performance. Notably, removing the Alignment module (w/o A) caused the most significant performance degradation, highlighting the importance of the prototype-guided latent space structure for learning a generalizable normative model.

5.3 Sensitivity Study

To validate our architectural choices and hyperparameter settings, we conducted a sensitivity analysis, with results presented in Figure 4.

First, we evaluated the impact of our Transformer-based backbone by comparing its performance against four other widely-used time-series encoders: LSTM, a standard CNN, EEGNet, and TCN. As shown in Figure 4a and 4b, the Transformer architecture achieves the best performance by a significant margin. It yields the lowest MAE of 2.645 and the lowest RMSE, substantially outperforming the next-best model, TCN, as well as EEGNet, CNN, and LSTM. This result confirms that the long-range dependency modeling of the Transformer is highly effective for this task and justifies its selection as our primary encoder.

Second, we analyzed the model’s sensitivity to the two key loss-weighting hyperparameters in our composite loss function: β (for L_{IB}) and γ (for L_{align}). For the β sensitivity test (Figure 4c), we evaluated values within {0.01, 0.02, 0.03, 0.04, 0.05, 0.06}. The model achieves its best performance with a small β (e.g., $\beta = 0.01$), with the MAE degrading as the VIB compression penalty increases, which justifies our selection of a small β value. For the γ sensitivity test (Figure 4d), we evaluated values within {0.1, 0.3, 0.5, 0.7, 0.9}. The plot shows a clear U-shaped curve: the MAE decreases from 3.2 at $\gamma = 0.1$, reaches its global minimum of 2.645 at $\gamma = 0.7$, and then rises again at $\gamma = 0.9$. This result demonstrates that the prototype alignment is critical for performance, but must be balanced against the primary prediction task, validating our final choice of $\gamma = 0.7$.

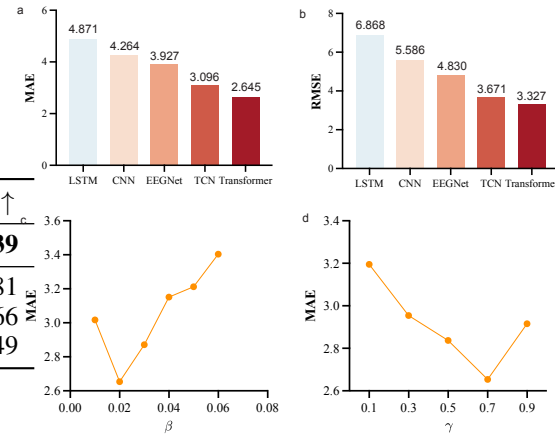


Figure 4: Sensitivity analysis of EVA-Net. (a, b) MAE and RMSE comparison across encoder backbones. (c) VIB loss weight β sensitivity within {0.01, 0.02, 0.03, 0.04, 0.05, 0.06}. (d) Prototype alignment loss weight γ sensitivity within {0.1, 0.3, 0.5, 0.7, 0.9}, optimal at $\gamma = 0.7$.

0.02, 0.03, 0.04, 0.05, 0.06}. The model achieves its best performance with a small β (e.g., $\beta = 0.01$), with the MAE degrading as the VIB compression penalty increases, which justifies our selection of a small β value. For the γ sensitivity test (Figure 4d), we evaluated values within {0.1, 0.3, 0.5, 0.7, 0.9}. The plot shows a clear U-shaped curve: the MAE decreases from 3.2 at $\gamma = 0.1$, reaches its global minimum of 2.645 at $\gamma = 0.7$, and then rises again at $\gamma = 0.9$. This result demonstrates that the prototype alignment is critical for performance, but must be balanced against the primary prediction task, validating our final choice of $\gamma = 0.7$.

5.4 Anomaly Detection on Pathological Cohorts

Having established EVA-Net’s state-of-the-art regression performance on the healthy cohort, we tested our core hypothesis: that the learned normative manifold can serve as an effective anomaly detector for pathological aging. We froze the trained model and applied it to the unseen pathological cohort (12 MCI and 15 AD subjects).

As defined in our Evaluation Metrics, we computed both the Brain-Age Gap (BAG) and the Prototype Alignment Error (PAE) for all subjects. The distributions of these anomaly scores are visualized in Figure 5. As shown, the healthy test subjects exhibited a minimal BAG (0.2 ± 3.3

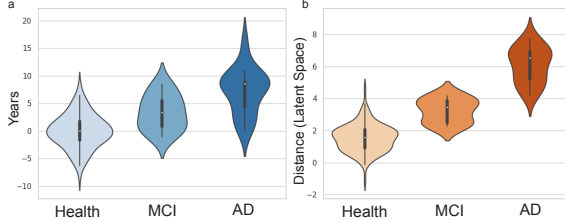


Figure 5: Violin plots illustrating the distribution of anomaly scores across cohorts. (a) Brain-Age Gap (BAG): While the healthy control group ($N=130$) is centered around zero, the MCI ($N=12$) and AD ($N=15$) groups show progressively larger positive gaps, indicating accelerated brain aging. (b) Prototype Alignment Error (PAE): A similar trend is observed for PAE, where pathological groups exhibit significantly larger distances from the normative manifold. The violin shapes visualize the full density of the data, highlighting the clear separation between healthy and pathological distributions.

years) and a low baseline PAE (1.5 ± 0.8), confirming that the model accurately maps healthy individuals to the normative manifold. In contrast, the pathological groups demonstrated progressive distributional shifts away from the healthy norm. The MCI group showed a significantly elevated mean BAG of 3.7 ± 3.1 years and a PAE of 3.1 ± 1.2 . The AD group exhibited the most severe deviation, with a mean BAG reaching 7.4 ± 4.5 years and a PAE of 5.6 ± 1.7 . These results confirm a clear trend ($AD > MCI > Healthy$) where disease severity strongly correlates with the magnitude of deviation from the learned healthy prototype, validating PAE as a sensitive, interpretable marker for pathology.

6 Conclusion

In this work, we presented EVA-Net, a novel framework for normative brain-age modeling and anomaly detection from imperfect, healthy-only EEG data. By integrating an efficient ProbSparse attention backbone, a Variational Information Bottleneck, and an age-conditioned continuous prototype network, EVA-Net successfully learns a robust, compressed, and geometrically interpretable manifold of healthy aging. Our extensive experiments demonstrate that EVA-Net not only achieves state-of-the-art regression accuracy on healthy subjects (MAE of 2.645 years) but also serves as a powerful anomaly detector. The proposed Prototype Alignment Error (PAE) effectively quantified pathological deviations in unseen MCI and AD cohorts, revealing a clear progression of disease severity. This study establishes a new, interpretable paradigm for leveraging deep learning on widely available clinical EEG data to screen for neurodegenerative conditions, paving the way for low-cost, accessible brain health monitoring.

Acknowledgment

This work was supported by the National Natural Science Foundation of China (Grant No. 81702469) and the Natural Science Foundation of Shandong Province (Grant No. ZR2023MH321).

This work involved human subjects in its research. Approval of all ethical and experimental procedures and protocols was granted by the Ethics Committee of Qilu Hospital of Shandong University under Protocol No. KYLL-202406 (YJ) -010.

References

- [1] Han Peng, Weikang Gong, Christian F Beckmann, Andrea Vedaldi, and Stephen M Smith. Accurate brain age prediction with lightweight deep neural networks. *Medical Image Analysis*, 68:101871, 2021.
- [2] Jiook Lee, Benjamin J Burkett, Hoon-Ki Min, Matthew L Senjem, Emily S Lundt, Hugo Botha, Jonathan Graff-Radford, Jeffrey L Gunter, Christopher G Schwarz, et al. Deep learning-based brain age prediction in normal aging and dementia. *Nature Aging*, 2(5):412–424, 2022.
- [3] Ann-Marie G de Lange, Melis Anatürk, Jaroslav Röckicki, Laura KM Han, Katja Franke, Dag Alnæs, Klaus P Ebmeier, Bogdan Draganski, Tobias Kauffmann, Lars T Westlye, et al. Mind the gap: Performance metric evaluation in brain-age prediction. *Human Brain Mapping*, 43(10):3113–3129, 2022.
- [4] Siuly Siuly, Yan Li, and Yanchun Zhang. Eeg signal analysis and classification. *IEEE Transactions on Neural Systems and Rehabilitation Engineering*, 11:141–144, 2016.
- [5] SJM Smith. Eeg in the diagnosis, classification, and management of patients with epilepsy. *Journal of Neurology, Neurosurgery & Psychiatry*, 76(suppl 2):ii2–ii7, 2005.
- [6] Tomas Ros, Jean Théberge, Paul A Frewen, Renee Kluetsch, Maria Densmore, Vince D Calhoun, and Ruth A Lanius. Mind over chatter: plastic up-regulation of the fmri salience network directly after eeg neurofeedback. *Neuroimage*, 65:324–335, 2013.
- [7] Yannick Roy, Hubert Banville, Isabela Albuquerque, Alexandre Gramfort, Tiago H Falk, and Jocelyn Faubert. Deep learning-based electroencephalography analysis: A systematic review. *Journal of Neural Engineering*, 16(5):051001, 2019.
- [8] Yicheng Liu, Lina Qin, Xiaogang Chen, Regine Le Bouquin Jeannes, Jean Louis Coatrieux, and Huazhong Shu. Advancing cross-subject domain generalization in brain-computer interfaces with multi-adversarial strategies. *IEEE Transactions on Instrumentation and Measurement*, 2025.

- [9] Kunyu Zhang, Liyue Gu, Lei Liu, Yuxuan Chen, Bairu Wang, Junjie Yan, and Yongfeng Zhu. Clinical expert uncertainty guided generalized label smoothing for medical noisy label learning. *arXiv preprint arXiv:2508.02495*, 2025.
- [10] Shuoyan Li, Madeline Malamut, Ann McKee, Jonathan D Cherry, and Lu Tian. Age-informed, attention-based weakly supervised learning for neuropathological image assessment. *Brain Informatics*, 12(1):27, 2025.
- [11] Tianchen Gao, Dexuan Chen, Mingyang Zhou, Yingying Wang, Yongchao Zuo, Wenxin Tu, Xinlin Li, and Junqi Chen. Self-training eeg discrimination model with weakly supervised sample construction: An age-based perspective on asd evaluation. *Neural Networks*, 187:107337, 2025.
- [12] Xiang-Hao Liu, Yan-Kai Liu, Yansen Wang, Kan Ren, Hanwen Shi, Zizheng Wang, Dongsheng Li, Bao-Liang Lu, and Wei-Long Zheng. Eeg2video: Towards decoding dynamic visual perception from eeg signals. In *Advances in Neural Information Processing Systems*, volume 37, pages 72245–72273, 2024.
- [13] Yikai Zhang, Rongyao Xie, Iman Beheshti, Xingyu Liu, Guowei Zheng, Yinxia Wang, Zhipeng Zhang, Weihao Zheng, Zhijun Yao, and Bin Hu. Improving brain age prediction with anatomical feature attention-enhanced 3d-cnn. *Computers in Biology and Medicine*, 169:107873, 2024.
- [14] Ailin Deng and Bryan Hooi. Graph neural network-based anomaly detection in multivariate time series. In *Proceedings of the AAAI Conference on Artificial Intelligence*, volume 35, pages 4027–4035, 2021.
- [15] Iman Beheshti, Mudasir A Ganaie, Vinay Paliwal, Amit Rastogi, Imran Razzak, and M Tanveer. Predicting brain age using machine learning algorithms: A comprehensive evaluation. *IEEE Journal of Biomedical and Health Informatics*, 26(4):1432–1440, 2021.
- [16] Ashish Vaswani, Noam Shazeer, Niki Parmar, Jakob Uszkoreit, Llion Jones, Aidan N Gomez, Łukasz Kaiser, and Illia Polosukhin. Attention is all you need. In *Advances in Neural Information Processing Systems*, volume 30, 2017.
- [17] Peyman Hosseinzadeh Kassani, Alexej Gossmann, and Yu-Ping Wang. Multimodal sparse classifier for adolescent brain age prediction. *IEEE Journal of Biomedical and Health Informatics*, 24(2):336–344, 2019.
- [18] Anees Abrol, Vince D Calhoun, Alzheimer’s Disease Neuroimaging Initiative, et al. Generating mri-derived csf proxy-markers to predict and visualize alzheimer’s disease progression. *Human Brain Mapping*, 46(16):e70391, 2025.
- [19] Yixin Wei, Anees Abrol, James Lah, Allan I Levey, and Vince D Calhoun. From symptomatic to pre-symptomatic: Adaptive knowledge distillation for early alzheimer’s detection using functional mri. *IEEE Transactions on Biomedical Engineering*, 2025.
- [20] Jie Wang, Yu Zhang, Zhe Song, and Tao Cheng. Bigdc-brainagenet: Enhancing eeg-based brain age prediction with bidirectional graph diffusion convolutions. In *Proceedings of International Symposium on Bioinformatics Research and Applications*, pages 320–332, 2025.
- [21] Xiaoran Shan, Jian Cao, Shuai Huo, Lu Chen, Ptolemaios G Sarrigiannis, and Yifan Zhao. Spatial-temporal graph convolutional network for alzheimer classification based on brain functional connectivity imaging of electroencephalogram. *Human Brain Mapping*, 43(17):5194–5209, 2022.
- [22] Xin Wu, Xinyu Ju, Shichao Dai, Xiaoli Li, and Ming Li. Multi-source domain adaptation for eeg emotion recognition based on inter-domain sample hybridization. *Frontiers in Human Neuroscience*, 18:1464431, 2024.
- [23] Yong-Eun Lee and Seong-Hu Lee. Eeg-transformer: Self-attention from transformer architecture for decoding eeg of imagined speech. In *Proceedings of 10th International Winter Conference on Brain-Computer Interface (BCI)*, pages 1–4. IEEE, 2022.
- [24] Guichun Wang, Wei Liu, Yihao He, Chenxi Xu, Li Ma, and Haoxing Li. Eegpt: Pretrained transformer for universal and reliable representation of eeg signals. In *Advances in Neural Information Processing Systems*, volume 37, pages 39249–39280, 2024.
- [25] Lukas AW Gemein, Robin Tibor Schirrmeister, Joschka Boedecker, and Tonio Ball. Brain age revisited: Investigating the state vs. trait hypotheses of eeg-derived brain-age dynamics with deep learning. *Imaging Neuroscience*, 2:1–22, 2024.
- [26] Meike Nauta, Jörg Schlötterer, Maurice Van Keulen, and Christin Seifert. Pip-net: Patch-based intuitive prototypes for interpretable image classification. In *Proceedings of IEEE/CVF Conference on Computer Vision and Pattern Recognition*, pages 2744–2753, 2023.
- [27] Yuchen Wang, Kunyu Zhang, Jin Huang, Nan-jun Yin, Siyuan Liu, and Eran Segal. Protomol: Enhancing molecular property prediction via prototype-guided multimodal learning. *arXiv preprint arXiv:2510.16824*, 2025.
- [28] Naftali Tishby and Noga Zaslavsky. Deep learning and the information bottleneck principle. In *Proceedings of IEEE Information Theory Workshop (ITW)*, pages 1–5. IEEE, 2015.
- [29] Sijie Hu, Zhiqiang Lou, Xiangyun Yan, and Yapeng Ye. A survey on information bottleneck. *IEEE Transactions on Pattern Analysis and Machine Intelligence*, 46(8):5325–5344, 2024.

- [30] Kunyu Zhang, Qiang Li, and Siwei Yu. Mvhō-ib: Multi-view higher-order information bottleneck for brain disorder diagnosis. In *Proceedings of International Conference on Medical Image Computing and Computer-Assisted Intervention*, pages 407–417, 2025.
- [31] Alexander A Alemi, Ian Fischer, Joshua V Dillon, and Kevin Murphy. Deep variational information bottleneck. *arXiv preprint arXiv:1612.00410*, 2016.
- [32] Hong Li, Chenglu Zhu, Yunlong Zhang, Yuxuan Sun, Zhongyi Shui, Wenlong Kuang, Sunyi Zheng, and Lin Yang. Task-specific fine-tuning via variational information bottleneck for weakly-supervised pathology whole slide image classification. In *Proceedings of IEEE/CVF Conference on Computer Vision and Pattern Recognition*, pages 7454–7463, 2023.
- [33] Arnaud Attyé, François Renard, Valérie Anglade, Alexandre Krainik, Philippe Kahane, Boris Mansencal, Pierrick Coupé, and Fernando Calamante. Data-driven normative values based on generative manifold learning for quantitative mri. *Scientific Reports*, 14(1):7563, 2024.
- [34] Vernon J Lawhern, Amelia J Solon, Nicholas R Waytowich, Stephen M Gordon, Chou P Hung, and Brent J Lance. Eegnet: a compact convolutional neural network for eeg-based brain–computer interfaces. *Journal of Neural Engineering*, 15(5):056013, 2018.
- [35] Pradeep Hewage, Ardhendu Behera, Marcello Trovati, Ella Pereira, Morteza Ghahremani, Francesco Palmieri, and Yonghuai Liu. Temporal convolutional neural (tcn) network for an effective weather forecasting using time-series data from the local weather station. *Soft Computing*, 24(21):16453–16482, 2020.
- [36] Hongseok Yu, Sungho Baek, Junhyuk Lee, Illsoo Sohn, Boreom Hwang, and Cheolsoo Park. Deep neural network-based empirical mode decomposition for motor imagery eeg classification. *IEEE Transactions on Neural Systems and Rehabilitation Engineering*, 32:3647–3656, 2024.
- [37] Huiyun Pan, Yurui Wang, Zengwei Li, Xuefei Chu, Bo Teng, and Hongzhi Gao. A complete scheme for multi-character classification using eeg signals from speech imagery. *IEEE Transactions on Biomedical Engineering*, 71(8):2454–2462, 2024.
- [38] Obada Al Zoubi, Chung Ki Wong, Rayus T Kuplicki, Hung-wen Yeh, Ahmad Mayeli, Hazem Refai, Martin Paulus, and Jerzy Bodurka. Predicting age from brain eeg signals—a machine learning approach. *Frontiers in Aging Neuroscience*, 10:184, 2018.
- [39] Yixin Jiang, Yuhang Mu, Zhenyu Xu, Qingqing Liu, Shuai Wang, Hao Wang, and Jia Feng. Identifying individual brain development using multimodality brain network. *Communications Biology*, 7(1):1163, 2024.